Dalton Transactions

ROYAL SOCIETY OF CHEMISTRY

PAPER

View Article Online
View Journal | View Issue

Cite this: *Dalton Trans.*, 2025, **54**, 6156

1-Amino-5-nitriminotetrazolate as a promising anion in safe yet powerful energetic coordination compounds†

Maximilian Benz,[a] Simon M. J. Endraß,[a,b] Thomas M. Klapötke,[a,b] Jörg Stierstorfer *[a,b] and Sadiq Strey[a]

Received 13th January 2025,
Accepted 4th March 2025

DOI: 10.1039/d4dt03086a

rsc.li/dalton

Ammonium 1-amino-5-nitriminotetrazolate (NH_4ANIT) was used as a precursor for energetic coordination compounds (ECCs). The highly energetic copper salt $[Cu(ANIT)_2(H_2O)_2]$ was selectively prepared. The reaction of NH_4ANIT with copper(II) nitrate trihydrate followed by the addition of neutral ligands (L), such as 1,2-di(1*H*-tetrazol-1-yl)ethane (1,1-dte), 1,3-di(1*H*-tetrazol-1-yl)propane (1,1-dtp), and 1-(2-azidoethyl)-1*H*-tetrazole (1-AET), produced energetic complexes of the types $[Cu(ANIT)_2(L)_2]$ and $[Cu(ANIT)_2(\mu\text{-}L)]$. The structural characteristics of these ECCs were analyzed by low temperature single crystal X-ray diffraction analysis. Their energetic parameters, such as impact and friction sensitivities according to BAM, were evaluated to give insight into the value of the ANIT anion for replacements of the commercially used lead azide (LA) and lead styphnate (LS) as primary explosives. The two most promising candidates $[Cu(ANIT)_2(H_2O)_2]$ and $[Cu(ANIT)_2(1\text{-}AET)_2]$ were analyzed concerning their particle distribution and sphericity by laser diffraction particle size analysis and scanning electron microscopy to gain insight into the processability of these substances.

Introduction

The ecological effects of the use of blasting are gaining significant importance in the field of energetic materials. For a long time, the intention of developing new energetic materials was mainly driven by academic interests combined with the military demand for improving their performance.[1] Nowadays, industrial demand is also increasing due to legislation and the awareness of the negative effects that the released compounds have.[2–4] In particular, the effects of lead distributed in soil and water through the use of lead azide (LA) and lead styphnate (LS) as primary explosives have to be considered.[5,6] Alongside the reliability and ecological impact, personal safety of the operating staff plays a crucial role in the production, transport and handling of explosives.[7] One way of reducing the amount of toxic waste released during blasting is to replace LA and LS with compounds that do not share the heavy metal toxicity of lead. One approach for accomplishing this goal is the use of energetic coordination compounds (ECCs). These ECCs benefit from the use of less toxic metals such as copper and iron, while compensating for the loss of density by incorporating highly energetic ligands and anions. To be considered green alternatives, their central metal should exhibit as little toxicity as possible. Furthermore, the anions and ligands should ideally be non-toxic and have a straightforward synthesis.

By applying nitrogen-rich ammonium 1-amino-5-nitriminotetrazolate (NH_4ANIT) as a precursor substance for the synthesis, the ANIT anion can be introduced into the world of ECCs. This creates the option to produce ECCs of the types $[Cu(ANIT)_2(L)_2]$ and $[Cu(ANIT)_2(\mu\text{-}L)]$ (Fig. 1).

By using the chelating ANIT anion, ECCs with lower solubility in water should be obtained. Similar approaches have recently been reported in several publications, which rely on the chelating effect of aromatic hydrazides as ligands.[10–12] Compared to the recently studied ECCs, the compounds presented in this work do not rely on typical oxidizing anions like chlorate, perchlorate, bromate or nitroaromatic anions, which are known for their toxicity.[12–17] Furthermore, existing 5-nitriminotetrazolates with different substituents apart from the amino group could be used in a similar manner.[18,19] This would further increase the variability of the ECC concept, as previous publications focused more on the acidic character of 5-nitriminotetrazolates, resulting in the formation of salts and ECCs with aqua-ligands.[8,19–21]

[a]*Department of Chemistry, Ludwig-Maximilians-Universität München, Butenandtstr. 5-13, 81377 Munich, Germany. E-mail: jstch@cup.uni-muenchen.de*
[b]*EMTO GmbH, Energetic Materials Technology, 81477 Munich, Germany*

† Electronic supplementary information (ESI) available. CCDC 2394591, 2394593, 2394588, 2394623, 2394590, 2394592, 2394589 and 2394622. For ESI and crystallographic data in CIF or other electronic format see DOI: https://doi.org/10.1039/d4dt03086a

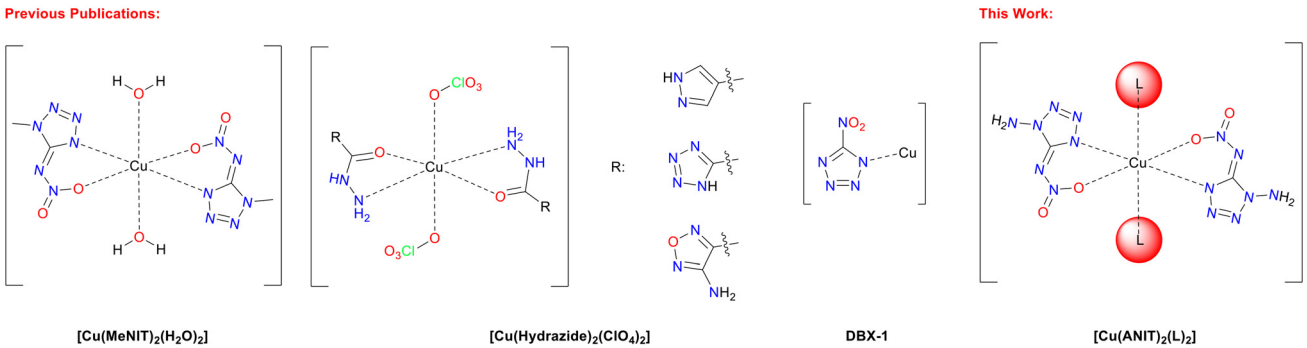

Fig. 1 Schematic drawing of $[Cu(ANIT)_2(L)_2]$ compared to DBX-1 and previously published ECCs with chelating ligands.[8–12]

As a comparable compound, which also aims for a reduction of environmental damage, copper(I) 5-nitrotetrazolate (DBX-1) was selected. While the simple composition of DBX-1 looks very promising, the need for very clean sodium nitrotetrazolate as a precursor can be considered as a drawback in terms of processing safety, as it requires the intermediate formation of diazoniumtetrazolate.[9,13,22,23] This intermediate species can reportedly undergo microdetonations within solution.[24,25]

This work seeks to introduce copper(II) and iron(II) 1-amino-5-nitriminotetrazolate-based coordination compounds as primary explosives with mechanical stability that exceeds commercially used LA and LS.

Results and discussion

Synthesis

NH_4ANIT was chosen as a bench-stable precursor substance. Its higher thermal stability ($T_{dec.}$: 185 °C) and resistance to friction (20 N) compared to the neutral HANIT ($T_{dec.}$: 145 °C, FS: 5 N) allow for safer handling.[26] Its synthesis, starting from 1,5-DAT, is shown in Scheme 1. Protection of the sp^3-hybridized amino group is necessary due to higher reactivity. After nitration with N_2O_5, the protection group is cleaved during quenching in iced water. As reported in the literature, nitration under protic conditions is not feasible due to the lability of the protection group.[26] The formation of NH_4ANIT is then performed with ethanolic ammonia.

The complexation was then conducted as shown in Scheme 2. Ammonium 1-amino-5-nitriminotetrazolate (NH_4ANIT), was synthesized according to Benz *et al.*[26] By dissolving NH_4ANIT in water at 60 °C and adding $Cu(NO_3)_2{\cdot}3H_2O$, an aqueous solution of $[Cu(ANIT)_2(H_2O)_2]$ (**1**) can be obtained. Using only small amounts of water as a solvent hereby leads to the precipitation of **1** with a yield of 52%. By the addition of another aqueous solution of the respective ligand to a solution of **1**, the aqua-ligands can be exchanged for nitrogen-rich ligands with high heat of formation. Crystallization at room temperature then allowed for the formation of the ECCs **2–8**, except for **5a**. To evaluate the value of the ANIT anion for

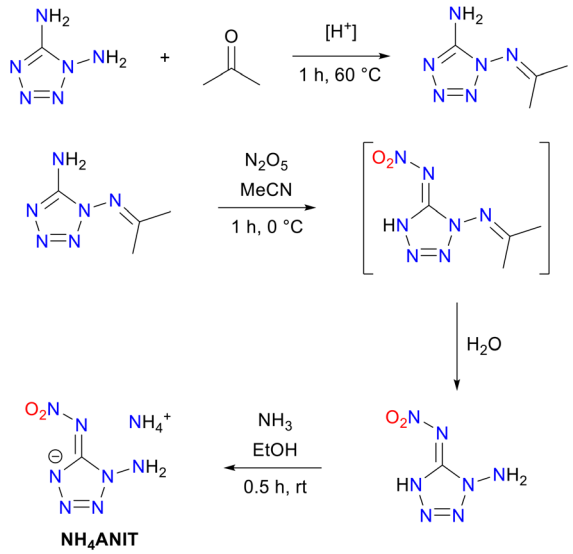

Scheme 1 Synthesis of NH_4ANIT as a precursor for ECCs.

ECCs, complexation attempts were carried out with several neutral ligands. In some cases with more polar ligands such as ammonia, 1-methyl-tetrazole, 1- and 2-amino-tetrazole, as well as 1-nitratomethyl-tetrazole, either no solid compounds were obtained or the elemental analyses differed from the values of the expected products. One possible contamination observed in these cases was $[Cu(ANIT)_2(H_2O)_2]$ (**1**), which was confirmed by single crystal X-ray diffraction analysis. Successful complexation was obtained in the cases of the ligands shown in Fig. 2. While ethylenediamine (en) was purchased from Sigma Aldrich, 1,2-di(1*H*-tetrazol-1-yl)ethane (1,1-dte), 1,3-di(1*H*-tetrazol-1-yl)propane (1,1-dtp), 1,4-di(1*H*-tetrazol-1-yl)butane (1,1-dtb), 2-(1*H*-tetrazol-1-yl)ethyl nitrate (1-NET), 1-(2-azidoethyl)-1*H*-tetrazole (1-AET) and 1-(3-azidopropyl)-1*H*-tetrazole (1-APT) were synthesized according to the literature.[27–32]

By changing the procedure to general procedure B, precipitation of **3–8**, excluding **5b**, was successfully achieved. Therefore, NH_4ANIT and the respective ligand were dissolved together at 60 °C in less solvent. In these cases, a solution of $CuSO_4{\cdot}5H_2O$ was added dropwise. Precipitation occurred

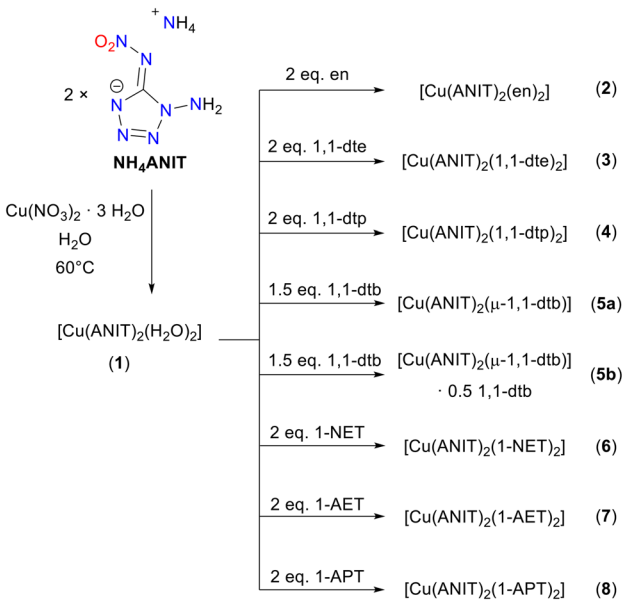

Scheme 2 Successful complexation attempts with NH_4ANIT as a starting material.

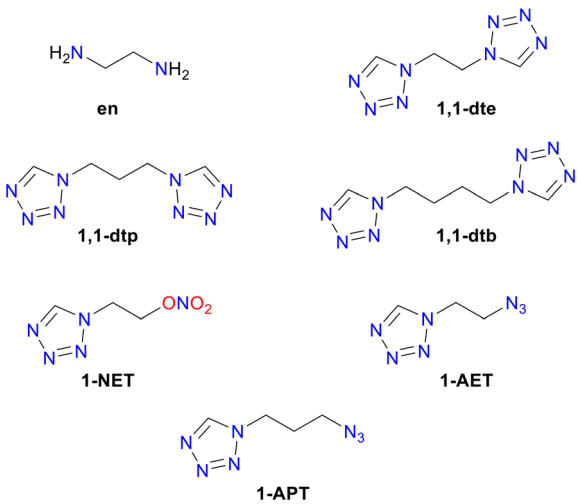

Fig. 2 Ligands used to prepare ECCs with the ANIT anion.

during the addition or upon stirring for a few minutes, resulting in the product with increased flowability.

By applying the procedure for precipitation to $FeSO_4 \cdot 1.5H_2O$, $[Fe(ANIT)_2(H_2O)_2] \cdot 2H_2O$ was obtained (Scheme 3) in a yield of 68% within 10 minutes. The exact procedure is given in the experimental section. Similar attempts with $Fe(NO_3)_3 \cdot 9H_2O$, $MnSO_4 \cdot 4H_2O$ and $Zn(NO_3)_2 \cdot 6H_2O$ did not result in solid products or impure compounds, as indicated by elemental analysis in attempts with the abovementioned ligands.

Crystal structures

All crystalline products were analyzed by low-temperature X-ray diffraction analysis. The structures were solved in the Olex2

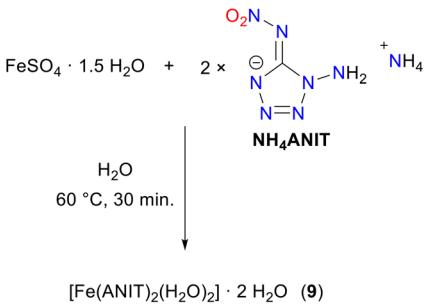

Scheme 3 Precipitation of $[Fe(ANIT)_2(H_2O)_2] \cdot 2H_2O$ (**9**).

software suite[33] using SHELXT[34] and refined using full-matrix least squares method on F^2 by SHELXL.[35,36] Figures of the crystal structures were created using DIAMOND4[37] displaying non-hydrogen atoms as thermal ellipsoids at a 50% probability level. Hydrogen atoms are shown as small spheres of arbitrary radius. Deposition numbers 2394591 (for **1**), 2394593 (for **3**), 2394588 (for **4**), 2394623 (for **5a**), 2394590 (for **5b**), 2394592 (for **7**), 2394589 (for **8**), and 2394622 (for **9**)† contain the supplementary crystallographic data for this paper.

Single crystals suitable for X-ray diffraction analysis of $[Cu(ANIT)_2(H_2O)_2]$ (**1**) can be obtained by evaporation of the aqueous solution at room temperature. The structure, as seen in Fig. 3 consists of two almost planar units of ANIT, coordinating to the copper(II) center. The torsion angle between the tetrazole and the nitrimine (N7–N6–C1–N4) can be determined to be 4.27(17)°. The elongated z^2-axis is occupied by two molecules of water. Hydrogen bonding between the ANIT anion and the water ligands results in alternating zigzag stacked layers of **1** as seen in Fig. 3b.

By replacing the water units of **1** by ligands, with stronger coordination to the metal center, the nitro group of the ANIT anion is pushed out of the plane of the ring. The *xy* plane in $[Cu(ANIT)_2(1,1\text{-dte})_2]$ (**3**) is therefore fully occupied by tetrazole rings, leaving only the z^2-orbital for coordination with nitrimine (Fig. 4). This results in an increased torsion angle of −13.4(2)° between the tetrazole ring and the nitrimine (N7–N6–C1–N4). Surprisingly, the typical crosslinking characteristics of di(1*H*-tetrazol-1-yl)alkane-ligands did not lead to bridging between the copper(II) centers and therefore the desired decrease of water-solubility. In contrast, using one equivalent of ligand resulted in impure samples, which can be explained by the crystallization of **1** along with the desired ECCs.

The incorporation of a ligand with higher steric demand, such as 1,1-dtp leads to yet another increase of the torsion angle N7–N6–C1–N4 to 20.6(5)° in $[Cu(ANIT)_2(1,1\text{-dtp})_2]$ (**4**) (Fig. 5). This results in a significantly longer Cu1–O1 bond of 2.408(2) Å compared to 2.2842(11) Å in **3**.

Unlike 1,1-dte and 1,1-dtp, 1,1-dtb manages to bridge two copper(II) centers, forming 1D-polymeric chains (Fig. 6 and 7). While precipitation results in **5a**, which does not incorporate additional ligands, slow evaporation allows for the formation of **5b**. By recrystallization of **5a** from small amounts of water,

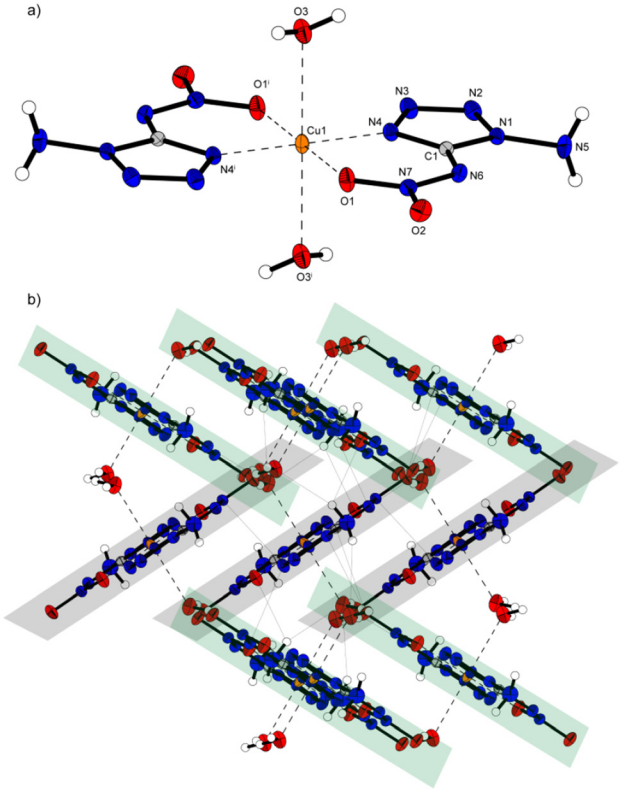

Fig. 3 Crystal structure of (a) the coordination sphere of [Cu(ANIT)$_2$(H$_2$O)$_2$] (**1**) and (b) a representation of its zigzag layers. Selected bond lengths [Å]: Cu1–O1 2.0206(16), Cu1–O3 2.3996(19), and Cu1–N4 1.9200(16). Selected bond angles [°]: O1–Cu1–O3 93.25(4), O1–Cu1–N4 85.57(4), and O3–Cu1–N4 90.02(4). Symmetry codes: (i) 1 – *x*, 1 – *y*, 1 – *z*.

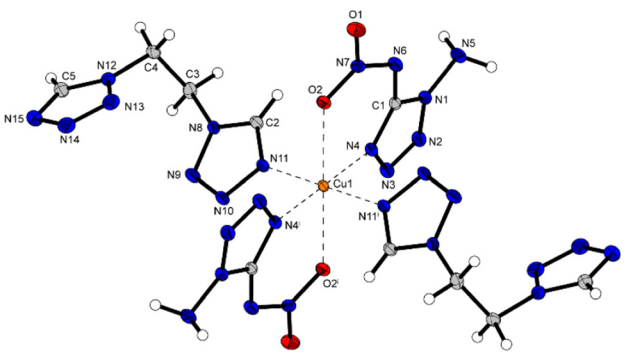

Fig. 4 Crystal structure of [Cu(ANIT)$_2$(1,1-dte)$_2$] (**3**). Selected bond lengths [Å]: Cu1–O2 2.2842(11), Cu1–N4 1.9754(12), and Cu1–N11 2.0390(12). Selected bond angles [°]: O2–Cu1–N4 77.21(4), O2–Cu1–N11 88.76(4), and N4–Cu1–N11 88.76(5). Symmetry codes: (i) –*x*, 1 – *y*, 1 – *z*.

single crystals suitable for X-ray diffraction analysis were obtained. The crystal structure shows that in **5a** 1,1-dtb not only coordinates *via* the N4 position of the tetrazole ring, but also *via* N3. This leads to a zigzag of alternatively coordinated copper(II) centers as demonstrated in Fig. 6(b).

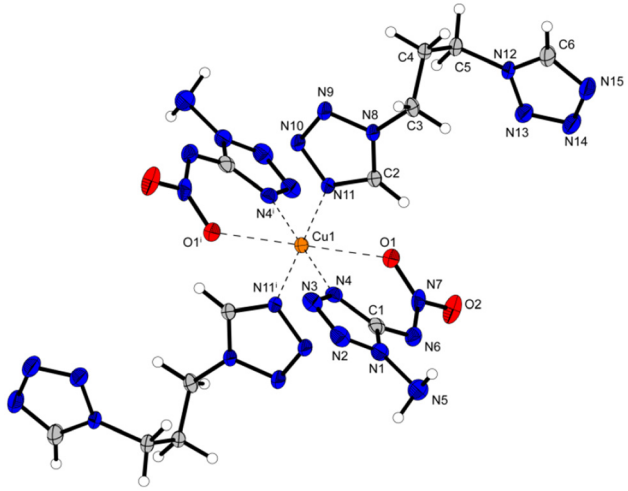

Fig. 5 Crystal structure of [Cu(ANIT)$_2$(1,1-dtp)$_2$] (**4**). Selected bond lengths [Å]: Cu1–O1 2.408(2), Cu1–N4 1.998(2), and Cu1–N11 2.001(2). Selected bond angles [°]: N11–Cu1–O1 87.66(9), N4–Cu1–O1 73.99(9), and N4–Cu1–N11 88.25(9). Symmetry codes: (i) 1 – *x*, –*y*, 2 – *z*.

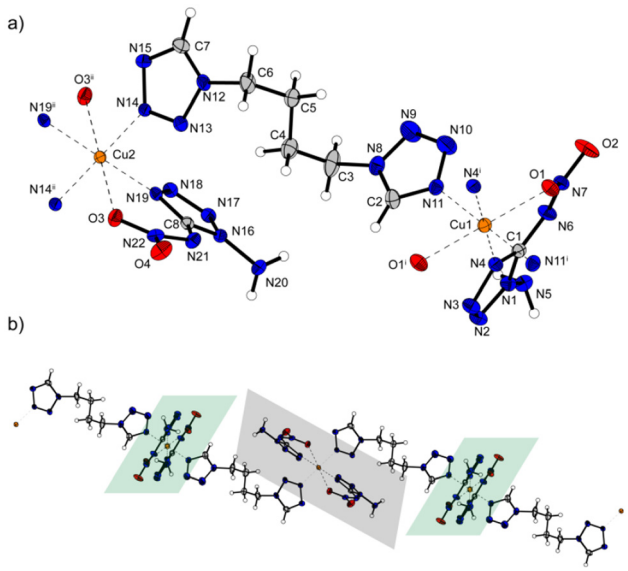

Fig. 6 Asymmetric unit of [Cu(ANIT)$_2$(μ-1,1-dtb)] (**5a**) (a) and polymeric representation (b). Selected bond lengths [Å]: Cu2–O3 2.3803(16), Cu2–N19 1.9857(18), Cu2–N14 2.0226(18), Cu1–O1 2.2906(15), Cu1–N11 2.0140(19), and Cu1–N4 1.988(2). Selected bond angles [°]: N19–Cu2–O3 74.79(7), N19–Cu2–N14 91.01(7), N14–Cu2–O3 92.55(7), N11–Cu1–O1 94.35(7), N4–Cu1–O1 78.06(7), and N4–Cu1–N11 87.37(8). Symmetry codes: (i) 1 – *x*, 2 – *y*, –*z*; (ii) –1 – *x*, 1 – *y*, 1 – *z*.

Unlike in **5a**, the polymeric chains of **5b** are solely formed by the coordination of the N4 of 1,1-dtb. When slowly crystallized with excess 1,1-dtb, these chains are connected with each other by hydrogen bonds between the ANIT amino group and N25, which belongs to a non-coordinating co-crystallized 1,1-dtb molecule. The distances between N25 and the two hydrogen atoms of the amino group are 2.5775 Å (H5A) and 2.5936 Å (H5B), respectively, allowing for interactions. The tetrazole rings of the non-

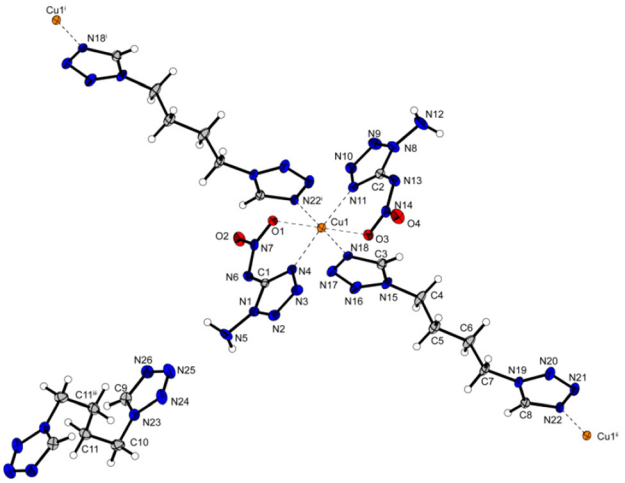

Fig. 7 Crystal structure of $[Cu(ANIT)_2(\mu\text{-}1,1\text{-dtb})]\cdot 0.5$ 1,1-dtb (**5b**). Selected bond lengths [Å]: Cu1–O1 2.3457(17), Cu1–O3 2.3592(18), Cu1–N22^i 2.0081(18), Cu1–N18 2.0038(18), Cu1–N4 1.9709(19), and Cu1–N11 1.9876(19). Selected bond angles [°]: O1–Cu1–O3 177.01(6), N22^i–Cu1–O1 87.70(7), N22^i–Cu1–O3 89.84(7), N18–Cu1–O1 91.52(7), N18–Cu1–O3 90.94(7), N18–Cu1–N22^i 179.22(9), N4–Cu1–O1 77.14(7), N4–Cu1–O3 101.15(7), N4–Cu1–N22^i 89.23(8), N4–Cu1–N18 90.54(7), N4–Cu1–N11 177.05(9), N11–Cu1–O1 105.71(7), N11–Cu1–O3 76.03(7), N11–Cu1–N22^i 91.64(7), and N11–Cu1–N18 88.64(8). Symmetry codes: (i) 1 – *x*, 1 – *y*, *z*; (ii) 1 + *x*, 1 + *y*, *z*; (iii) –*x*, –*y*, 2 – *z*.

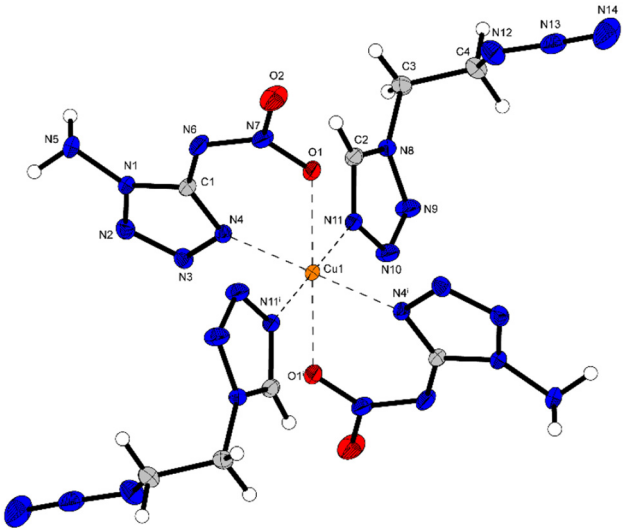

Fig. 8 Crystal structure of $[Cu(ANIT)_2(1\text{-AET})_2]$ (**7**). Selected bond lengths [Å]: Cu1–O1 2.3119(11), Cu1–N4 1.9823(12), and Cu1–N11 2.0147(13). Selected bond angles [°]: O1–Cu1–N4 76.75(5), O1–Cu1–N11 86.36(5), and N4–Cu1–N11 89.24(5). Symmetry codes: (i) 1 – *x*, 1 – *y*, 1 – *z*.

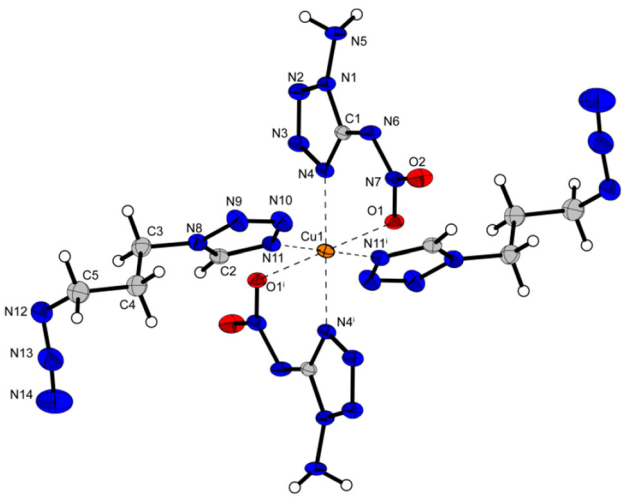

Fig. 9 Crystal structure of $[Cu(ANIT)_2(APT)_2]$ (**8**). Selected bond lengths [Å]: Cu1–O1 2.3308(14), Cu1–N11 2.0034(17), and Cu1–N4 1.9969(15). Selected bond angles [°]: N11–Cu1–O1 89.95(6), N4–Cu1–O1 77.17(6), and N4–Cu1–N11 89.89(7). Symmetry codes: (i) 1 – *x*, 1 – *y*, 1 – *z*.

coordinating 1,1-dtb furthermore show perfect coplanar stacking with the tetrazole rings of the ANIT anions.

The structural motif remains the same in the cases of $[Cu(ANIT)_2(1\text{-AET})_2]$ (**7**) (Fig. 8) and $[Cu(ANIT)_2(1\text{-APT})_2]$ (**8**) (Fig. 9). Similar to the di(1*H*-tetrazol-1-yl)alkane-ligands, the torsion angle N7–N6–C1–N4 increases in the case of the more sterically demanding ligand 1-APT (14.3(3)°) compared to 1-AET (12.7(3)°). Similarly, the z^2-axis is hereby elongated.

While **7** crystallized in the triclinic space group $P\bar{1}$, the crystallization of **8** occurs in the monoclinic space group $P2_1/n$. The direct comparison shows that the recalculated room temperature density decreases from 1.864 to 1.731 g cm^{-3} by increasing the chain length of the ligand from 1-AET to 1-APT.

Single crystals of $[Fe(ANIT)_2(H_2O)_2]\cdot 2H_2O$ (**9**) were obtained by letting the filtrate of the precipitation evaporate at room temperature. Interestingly, **9** did not crystallize in the usual pattern, which was observed for the $[Cu(ANIT)_2(L)_2]$-type. Cu(II) seems to favor coordination over the *N*4-position of the tetrazole ring, forming a six-membered ring with the nitro group. In **9**, however, coordination occurs *via* the amino group and the nitrimine's nitrogen to form five-membered rings. The crystal structure (Fig. 10) reveals, that this is accompanied by significantly longer distances between the Fe(II)-center and its ligands compared to the distances observed for **1**.

Energetic properties

Evaluations of the neutral compound HANIT and the precursor substance NH_4ANIT have been previously reported.[26] There is no doubt about the potential of ANIT as a highly energetic anion. Therefore, the substances produced in this work were characterized for their potential to serve as primary explosives. The thermal stabilities were measured by differential thermal analyses with an OZM DTA 551-ex. Endothermic signals were further investigated for mass loss with a PerkinElmer TGA4000 thermogravimetric analyzer and melting points with a Büchi B-540 device. The onset of the endothermic peak of $[Cu(ANIT)_2(H_2O)_2]$, observed at 87 °C in the DTA was confirmed by TGA to be the loss of the two aqua ligands. Interestingly, the differential thermal analysis of $[Cu(ANIT)_2(\mu\text{-}1,1\text{-dtb})]$ (**5a**) and

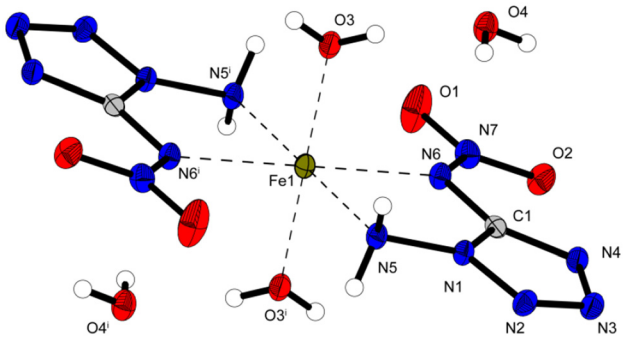

Fig. 10 Crystal structure of $[Fe(ANIT)_2(H_2O)_2]\cdot 2H_2O$ (**9**). Selected bond lengths [Å]: Fe1–O3 2.0649(10), Fe1–N5 2.2642(11), and Fe1–N6 2.1674 (11). Selected bond angles [°]: O3–Fe1–N5 90.31(4), O3–Fe1–N6 91.95 (4), and N6–Fe1–N5 76.63(4). Symmetry codes: (i) 2 – *x*, 1 – *y*, –*z*.

$[Cu(ANIT)_2(\mu\text{-}1,1\text{-dtb})]\cdot 0.5$ 1,1-dtb (**5b**) suggests, that the incorporation of the additional 1,1-dtb leads to a decrease of thermal stability. Impact and friction sensitivities were determined on BAM standard devices using the 1 of 6 method to evaluate the lowest impact energy or friction force at which one positive result occurs within six tests. The sensitivities against electrostatic discharge (ESD) were obtained with an OZM XSpark10 device. The mechanical sensitivities, which were observed, result in the classification of all compounds as very sensitive to impact and very sensitive or even extremely sensitive (**1**, **6** and **7**) to friction according to the UN Recommendations on the Transport of Dangerous Goods.[38] The surprisingly high sensitivity of **1** and **5a** (compared to **3**, **4** and **5b**) can be explained by their zigzag oriented coordination spheres. All other structures obtained show no signs of alternation of the orientation plane. The respective values can be found in Table 1. As first insights into the performances of the ECCs, hot plate (HP) and hot needle (HN) tests were performed as shown in Fig. 11. These tests provide information about the reaction of the substances towards rapid heating in both open

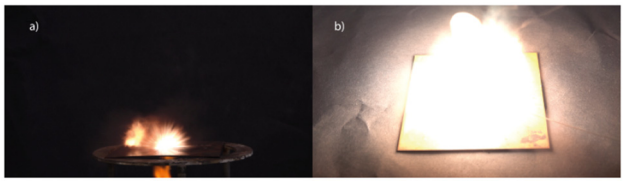

Fig. 11 (a) Hot plate and (b) hot needle tests of $[Cu(ANIT)_2(H_2O)_2]$ (**1**).

and confined environments. Obtaining a detonation or sharp deflagration in these tests can indicate the potential to initiate PETN in detonator setups.

For this reason, compounds **1** ($[Cu(ANIT)_2(H_2O)_2]$) **3,** ($[Cu(ANIT)_2(1,1\text{-dte})_2]$), **5a** ($[Cu(ANIT)_2(\mu\text{-}1,1\text{-dtb})]$), **7** ($[Cu(ANIT)_2(1\text{-AET})_2]$), **8** ($[Cu(ANIT)_2(1\text{-APT})_2]$) and **9** ($[Fe(ANIT)_2(H_2O)_2]\cdot 2H_2O$) were tested for their initiation capability. Therefore, 200 mg of PETN (<100 μm) was compressed into a copper detonator shell by dropping an 8 kg weight onto it. The shell was then placed on a copper witness plate, filled with the substance of interest (50/150 mg) and ignited by a type A electrical igniter. A schematic cross-section of the setup can be seen in Fig. 12. The test is considered positive in cases of penetration of the witness plate.

As **3**, **5a**, **7**, **8** and **9** did not manage to initiate the PETN charge successfully with 50 mg of the substance, the amounts were increased to 150 mg. This led to increased fragmentation and deformation of the shell in the cases of **3**, **5a** and **8**, without successful initiation. The outcome of the initiation test with **9** is not included in Fig. 13, as no change to the setup was visible. Only 150 mg of **7** managed to undergo a deflagration to detonation transition (DDT) and transmit this detonation to the PETN completely. This might be the result of the increased carbon content in $[Cu(ANIT)_2(1\text{-AET})_2]$ compared to $[Cu(ANIT)_2(H_2O)_2]$. While the sum formula of $[Cu(ANIT)_2(H_2O)_2]$ theoretically allows for full conversion of the compound into Cu, N_2, H_2O, and CO, $[Cu(ANIT)_2(1\text{-AET})_2]$

Table 1 Thermal stability and sensitivities of compounds **1**–**9** to external stimuli

Compound	No.	T_{endo}[a] [°C]	T_{exo}[b] [°C]	IS[c] [J]	FS[d] [N]	ESD[e] [mJ]	HP[f]	HN[g]	Initiation
$[Cu(ANIT)_2(H_2O)_2]$	**1**	87	219	<1	2.5	13	Det.	Def.	Pos.
$[Cu(ANIT)_2(en)_2]$	**2**	117	178	3	360	120	Def.	Dec.	—
$[Cu(ANIT)_2(1,1\text{-dte})_2]$	**3**	—	177	<1	30	200	Def.	Det.	Neg.[k]
$[Cu(ANIT)_2(1,1\text{-dtp})_2]$	**4**	—	167	<1	54	200	Def.	Def.	—
$[Cu(ANIT)_2(\mu\text{-}1,1\text{-dtb})]$	**5a**	—	169	<1	20	50	Det.	Det.	Neg.[k]
$[Cu(ANIT)_2(\mu\text{-}1,1\text{-dtb})]\cdot 0.5$ 1,1-dtb	**5b**	—	156	<1	54	50	Def.	Dec.	—
$[Cu(ANIT)_2(1\text{-NET})_2]$	**6**	—	151	<1	8	160	Def.	Def.	—
$[Cu(ANIT)_2(1\text{-AET})_2]$	**7**	—	159	<1	6	20	Def.	Det.	Pos.[k]
$[Cu(ANIT)_2(1\text{-APT})_2]$	**8**	—	167	<1	20	120	Def.	Det.	Neg.[k]
$[Fe(ANIT)_2(H_2O)_2]\cdot 2H_2O$	**9**	118[h]	118[h]	15	288	60	Det.	Dec.	Neg.[k]
DBX-1 [7,9]		—	330[i]	<1	<0.1	0.012[j]	Det.	Det.	Pos.
LA (RD-1333) [7,13,42]		—	320–350	4	≤0.1	0.007–5	Det.	Det.	Pos.

[a] Onset temperature of the endothermic event in the DTA (heating rate β = 5 °C min^{-1}), indicating a melting point of the compound. [b] Onset of the exothermic event in the DTA. [c] Impact sensitivity (BAM drophammer (1 of 6)). [d] Friction sensitivity (BAM friction tester (1 of 6)). [e] Electrostatic discharge device (OZM XSpark10). [f] Hot plate test (det.: detonation, def.: deflagration, dec.: decomposition, comb.: combustion). [g] Hot needle test (det.: detonation, def.: deflagration, dec.: decomposition, comb.: combustion). [h] Endo to exo transition. [i] β = 20 K min^{-1}. [j] Minimum fire level. [k] 150 mg of substance, 200 mg of PETN.

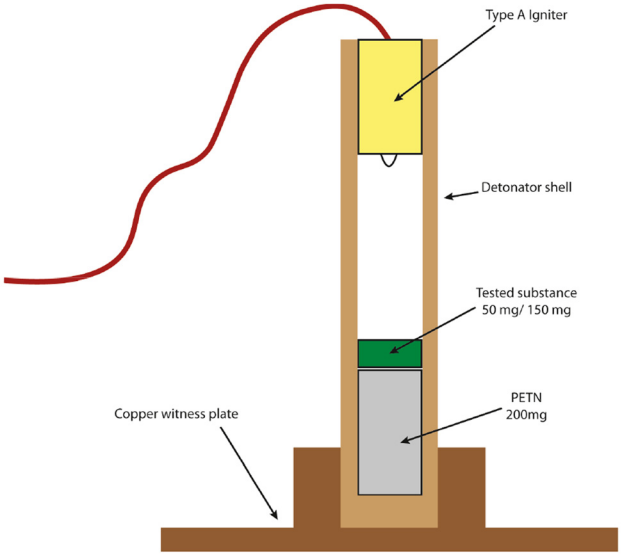

Fig. 12 Schematic diagram of the initiation test setup.

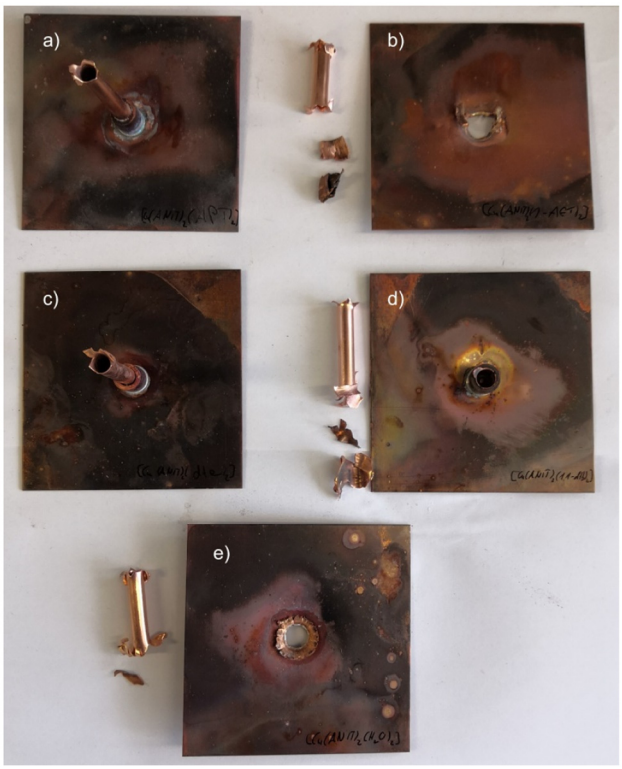

Fig. 13 Outcomes of the PETN initiation tests: (a) $[Cu(ANIT)_2(1\text{-}APT)_2]$ (**8**), (b) $[Cu(ANIT)_2(1\text{-}AET)_2]$ (**7**), (c) $[Cu(ANIT)_2(1,1\text{-}dte)_2]$ (**3**), (d) $[Cu(ANIT)_2(\mu\text{-}1,1\text{-}dtb)_2]$ (**5a**), and (e) $[Cu(ANIT)_2(H_2O)_2]$ (**1**).

shows a significant change in the fuel to oxidizer ratio. This balance of fuel to oxidizer has previously been shown to influence the potential of ECCs.[39–41]

Apart from the initiation capability and sensitivity of a substance, a major factor for its value is processability. The common technique of loading primary explosives volumetrically calls for a certain flowability of the substance.[43] A narrow particle size distribution, with low amounts of very fine particles and high sphericity contributes to this flowability.[44] Typically, very fine particles are removed during production by filtration of the product through grounded metal sieves of a certain mesh. This ensures the removal of very fine dust, which can negatively influence the powder properties, such as the sensitivity to electrostatic discharge, which is influenced by the particle size.[45] Furthermore, the particle sizes and shapes should be as reproducible as possible. The key advantage of production using a strategy for the precipitation of compounds **1** and **7** from the aqueous medium is the use of a non-toxic, non-flammable solvent. To investigate other impact factors of processability, the products of the precipitation attempts were analyzed in *i*-PrOH using a Microtrac SYNC particle size analyzer. Fig. 14 shows the particle size distribution of both compounds, revealing an even distribution of particles with a majority between 10 and 100 µm. Furthermore, these particles were detected to be mostly spherical, allowing a good flowability of the powder.

Fig. 15 shows scanning electron microscopy images of $[Cu(ANIT)_2(H_2O)_2]$ (**1**) at 120× (left), 700× (middle), and 3300× (right) magnification as well as $[Cu(ANIT)_2(1\text{-}AET)_2]$ (**7**) at 70× (left), 550× (middle), and 1200× (right) magnification. The

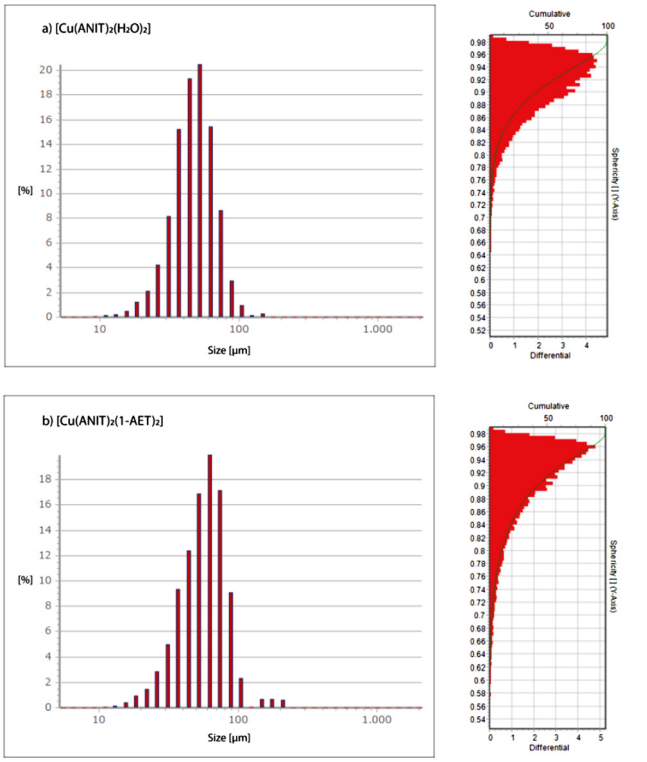

Fig. 14 Particle size measurement data obtained by Microtrac SYNC for (a) $[Cu(ANIT)_2(H_2O)_2]$ (**1**) (d_{10}: 24.63 µm, d_{50}: 52.98 µm, d_{90}: 94.72 µm) and (b) $[Cu(ANIT)_2(1\text{-}AET)_2]$ (**7**) (d_{10}: 23.36 µm, d_{50}: 46.37 µm, d_{90}: 79.07 µm).

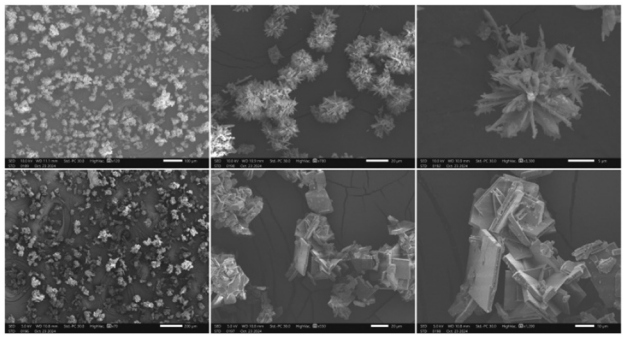

Fig. 15 Scanning electron microscopy images of $[Cu(ANIT)_2(H_2O)_2]$ (**1**) (top) and $[Cu(ANIT)_2(1\text{-AET})_2]$ (**7**) (bottom).

images reveal the nature of the primary particles during crystallization. Compound **1**, when precipitated according to the modified general procedure B consists of intergrown needles, which form spherical secondary particles that were observed in the particle size measurements. Compound **7** on the other hand can be precipitated according to general procedure B to form intergrown platelets. These again form secondary particles of a spherical nature. The full-sized images can be found in the ESI.†

Conclusions

In summary, nine new energetic coordination compounds, including the easily available and highly energetic anion 1-amino-5-nitriminotetrazolate were introduced and investigated concerning their physicochemical properties. Hereby, an important insight into the safety of handling of compounds of the type $[Cu(ANIT)_2(L)_2]$ is provided. Direct comparison with the commercially used lead azide, as well as the green alternative copper(I) nitrotetrazolate (DBX-1), shows that this type of ECC is mechanically more stable, yet of lower thermal stability. Similar to DBX-1, most ECCs presented in this work can be precipitated from aqueous solution. Performance tests revealed that the initiation of PETN is feasible with 150 mg of $[Cu(ANIT)_2(1\text{-AET})_2]$ and 50 mg of $[Cu(ANIT)_2(H_2O)_2]$. The observed high sphericity and even particle size distribution are good prerequisites for the processing of both compounds, as they allow even filling of the detonator shells.

Experimental section

Caution! All investigated compounds are energetic materials and some of them show sensitivity towards various stimuli (*e.g.* elevated temperatures, impact, friction or electronic discharge). Although no hazards occurred, suitable security precautions (safety glasses, face shield, earthed equipment and shoes, leather jacket, Kevlar sleeves, and earplugs) have to be worn while synthesizing and handling the described compounds.

General procedure A for the formation of $[Cu(ANIT)_2(H_2O)_2]$ (1) and ECCs 2–8

NH_4ANIT was prepared according to the literature.[26] 81.1 mg (0.50 mmol. 2.0 eq.) of NH_4ANIT was dissolved in water (10 mL) at 60 °C. $Cu(NO_3)_2{\cdot}3H_2O$ (60.4 mg, 0.25 mmol, 1.0 eq.) was then added to the solution, resulting in a change of color from yellow to green. ECCs **2–8** can be formed by the addition of a second aqueous solution (5 mL) of the respective ligand. After stirring at 60 °C for 10 min, the solutions can be transferred to a crystallization dish. After 4–7 days, the compounds of interest crystallized, and could be filtered off and washed with a small amount of cold H_2O and EtOH.

By allowing the solvent to evaporate at room temperature, instead of the addition of ligands, single crystals of **1** can be obtained. Crystals of **1** were also obtained by using small polar tetrazoles as ligands.

General procedure B for the precipitation of ECCs 3–9

To obtain the ECCs in a more homogeneous form, precipitation can be performed by first dissolving 81.1 mg (0.50 mmol. 2.0 eq.) of NH_4ANIT and the respective ligand in water (4 mL) at 60 °C. A solution of $CuSO_4{\cdot}5H_2O$ (62.4 mg, 0.25 mmol, 1.0 eq.) in 1 mL of water was then added dropwise under stirring for 10 minutes. Cooling to rt, while stirring for 20 minutes, leads to the precipitation of the ECC from the aqueous solution. The ECC can then be filtered off, and washed with small amounts of cold water, followed by EtOH and drying in air.

$[Cu(ANIT)_2(H_2O)_2]$ (1)

NH_4ANIT (81.1 mg, 0.50 mmol, 2.0 eq.) was dissolved in 3 mL of deionized water and stirred at 60 °C. A solution of $CuSO_4{\cdot}5H_2O$ (62.4 mg, 0.25 mmol, 1.0 eq.) in 1 mL of water was then added dropwise under stirring for 10 minutes. The solution was allowed to cool to room temperature and stirred for 30 min, during which precipitation of a luminous green solid occurred. The suspension was then filtered off, and washed with little water and EtOH before drying in air. This procedure yields 50.3 mg of **1** (0.13 mmol, 52%). **DTA** (5 °C min^{-1}) onset: 87 °C (endothermic), 219 °C (exothermic). **IR** (ATR, cm^{-1}): $\tilde{\nu}$ = 3452 (m), 3338 (w), 3287 (w), 3192 (w), 1622 (m), 1533 (m), 1491 (m), 1475 (m), 1394 (vs), 1336 (s), 1313 (vs), 1258 (vs), 1149 (m), 1116 (m), 1042 (m), 1014 (s), 898 (m), 881 (m), 776 (m), 756 (m), 730 (s), 707 (m), 685 (m), 549 (s), 529 (s), 484 (s), 425 (s), 411 (s), 404 (s). **EA** ($C_2H_8CuN_{14}O_6$, 387.72) calcd: C 6.20, H 2.08, N 50.58%; found: C 6.46, H 2.41, N 49.92%. **BAM drophammer**: <1 J. **Friction tester**: 2.5 N. **ESD**: 13 mJ (at a grain size of <100 μm).

$[Cu(ANIT)_2(en)_2]$ (2)

The addition of ethylenediamine (30.1 mg, 0.50 mmol, 2.0 eq.), dissolved in 5 mL of water to the aqueous solution of **1** (10 mL), led to intense purple discoloration. Compound **2** (36.6 mg, 0.08 mmol) was obtained in a yield of 32%. **DTA** (5 °C min^{-1}) onset: 117 °C (endothermic), 178 °C (exothermic).

IR (ATR, cm^{-1}): $\tilde{\nu}$ = 3320 (m), 3290 (m), 3278 (m), 3244 (m), 3220 (m), 3198 (m), 3156 (m), 2952 (w), 2901 (w), 1656 (w), 1626 (m), 1588 (m), 1508 (m), 1457 (m), 1436 (w), 1428 (w), 1411 (m), 1401 (m), 1383 (m), 1370 (s), 1307 (vs), 1287 (s), 1265 (vs), 1160 (m), 1107 (m), 1090 (m), 1042 (s), 1016 (s), 1005 (s), 983 (m), 960 (m), 883 (m), 823 (m), 778 (m), 729 (s), 706 (m), 701 (m), 679 (m), 544 (m), 531 (m), 521 (m), 475 (m), 461 (m), 418 (w). **EA** ($C_6H_{20}CuN_{18}O_4$, 471.89) calcd: C 15.27, H 4.27, N 53.43%; found: C 15.14, H 4.46, N 49.51%. **BAM drophammer**: 3 J. **Friction tester:** 360 N. **ESD**: 120 mJ (at a grain size of 100–500 μm).

[Cu(ANIT)$_2$(1,1-dte)$_2$] (3)

The addition of 1,2-di(1*H*-tetrazol-1-yl)ethane (83.1 mg, 0.50 mmol, 2.0 eq.), dissolved in 5 mL of water to the aqueous solution of **1** (10 mL), yielded **3** (133.6 mg, 0.20 mmol), which was obtained in a yield of 80%. **DTA** (5 °C min^{-1}) onset: 177 °C (exothermic). **IR** (ATR, cm^{-1}): $\tilde{\nu}$ = 3364 (w), 3095 (m), 1737 (m), 1627 (w), 1535 (w), 1508 (m), 1474 (m), 1458 (m), 1431 (m), 1421 (s), 1402 (s), 1380 (m), 1364 (m), 1334 (m), 1287 (s), 1236 (vs), 1192 (vs), 1174 (s), 1148 (s), 1106 (s), 1094 (vs), 1048 (m), 1012 (m), 999 (m), 970 (m), 947 (m), 926 (m), 910 (m), 891 (s), 843 (m), 797 (m), 769 (m), 763 (m), 726 (m), 705 (m), 688 (m), 670 (m), 657 (s), 640 (s), 529 (m), 491 (m), 473 (m). **EA** ($C_{10}H_{16}CuN_{30}O_4$, 683.99) calcd: C 17.56, H 2.36, N 61.44%; found: C 17.64, H 2.53, N 60.68%. **BAM drophammer**: <1 J. **Friction tester:** 30 N. **ESD**: 200 mJ (at a grain size of <100 μm).

[Cu(ANIT)$_2$(1,1-dtp)$_2$] (4)

The addition of 1,3-di(1*H*-tetrazol-1-yl)propane (90.1 mg, 0.50 mmol, 2.0 eq.) dissolved in 5 mL of water to the aqueous solution of **1** (10 mL), yielded **4** (122 mg, 0.17 mmol). **4** was obtained in a yield of 68%. **DTA** (5 °C min^{-1}) onset: 167 °C (exothermic). **IR** (ATR, cm^{-1}): $\tilde{\nu}$ = 3327 (w), 3214 (w), 3088 (w), 2987 (w), 1650 (vw), 1509 (m), 1465 (m), 1456 (m), 1445 (m), 1434 (m), 1414 (s), 1396 (m), 1350 (m), 1324 (m), 1284 (s), 1237 (s), 1190 (m), 1171 (s), 1162 (m), 1140 (m), 1104 (vs), 1044 (m), 1035 (m), 1019 (m), 1005 (m), 967 (m), 912 (m), 896 (m), 876 (m), 851 (m), 832 (m), 774 (m), 758 (m), 736 (m), 723 (w), 701 (m), 679 (w), 667 (m), 655 (m), 632 (m), 618 (m), 610 (m), 525 (w), 468 (m), 430 (m), 422 (w). **EA** ($C_{12}H_{20}CuN_{30}O_4$, 712.04) calcd: C 20.24, H 2.83, N 59.01%; found: C 20.30, H 3.01, N 58.77%. **BAM drophammer**: <1 J. **Friction tester:** 54 N. **ESD**: 200 mJ (at a grain size of <100 μm).

[Cu(ANIT)$_2$(μ-1,1-dtb)] (5a)

Using 1,4-di(1*H*-tetrazol-1-yl)butane (73.8 mg, 0.38 mmol, 1.5 eq.), precipitation according to General procedure B yielded **5a** (102.5 mg, 0.19 mmol, 76%). **DTA** (5 °C min^{-1}) onset: 169 °C (exothermic). **IR** (ATR, cm^{-1}): $\tilde{\nu}$ = 3313 (w), 3216 (w), 3188 (w), 3126 (w), 1640 (w), 1520 (m), 1512 (m), 1472 (m), 1460 (m), 1441 (m), 1418 (s), 1404 (s), 1367 (m), 1327 (s), 1290 (vs), 1254 (s), 1201 (m), 1191 (m), 1180 (m), 1148 (m), 1108 (s), 1083 (m), 1073 (m), 1016 (m), 1004 (m), 969 (m), 937 (m), 889 (m), 875 (m), 823 (w), 796 (m), 773 (m), 759 (m), 733 (m), 721 (w), 707 (w), 675 (m), 668 (m), 648 (m), 524 (w), 473 (m), 459 (m). **EA** ($C_8H_{14}CuN_{22}O_4$, 545.90) calcd: C 17.60, H 2.59, N 56.45%; found: C 17.74, H 2.92, N 55.62%. **BAM drophammer**: <1 J. **Friction tester**: 20 N. **ESD**: 50 mJ (at a grain size of <100 μm).

[Cu(ANIT)$_2$(μ-1,1-dtb)]·0.5 1,1-dtb (5b)

The addition of 1,4-di(1*H*-tetrazol-1-yl)butane (73.8 mg, 0.38 mmol, 1.5 eq.) dissolved in 5 mL of water to the aqueous solution of **1** (10 mL), yielded **5b** (104.0 mg, 0.16 mmol, 64%). **DTA** (5 °C min^{-1}) onset: 156 °C (exothermic). **IR** (ATR, cm^{-1}): $\tilde{\nu}$ = 3318 (m), 3312 (m), 3306 (m), 3280 (m), 3194 (w), 3128 (m), 1673 (w), 1641 (w), 1520 (m), 1513 (m), 1472 (m), 1460 (m), 1439 (m), 1417 (s), 1404 (s), 1367 (m), 1326 (s), 1289 (vs), 1254 (s), 1201 (m), 1190 (m), 1182 (m), 1148 (m), 1108 (s), 1082 (w), 1071 (w), 1043 (m), 1016 (m), 1004 (m), 939 (m), 888 (m), 828 (w), 797 (m), 773 (m), 760 (m), 733 (m), 721 (w), 707 (m), 675 (m), 668 (m), 647 (m), 526 (w), 472 (m), 462 (m), 456 (m), 439 (m), 428 (m), 424 (m), 419 (m). **EA** ($C_{22}H_{19}CuN_{26}O_4$, 642.99) calcd: C 20.55, H 2.98, N 56.64%; found: C 20.81, H 2.87, N 56.79%. **BAM drophammer**: <1 J. **Friction tester:** 54 N. **ESD**: 50 mJ (at a grain size of 100–500 μm).

[Cu(ANIT)$_2$(1-NET)$_2$] (6)

The addition of 2-(1*H*-tetrazol-1-yl)ethyl nitrate (79.6 mg, 0.50 mmol, 2.0 eq.), dissolved in 5 mL of water to the aqueous solution of **1** (10 mL), yielded **6** (123.0 mg, 0.18 mmol), which was obtained in a yield of 72%. **DTA** (5 °C min^{-1}) onset: 151 °C (exothermic). **IR** (ATR, cm^{-1}): $\tilde{\nu}$ = 3367 (w), 3217 (w), 3138 (w), 1634 (s), 1520 (m), 1506 (m), 1463 (m), 1450 (m), 1434 (m), 1397 (s), 1366 (m), 1337 (m), 1287 (vs), 1242 (vs), 1180 (s), 1171 (s), 1102 (s), 1073 (w), 1064 (w), 1026 (m), 1013 (m), 981 (m), 883 (s), 849 (s), 770 (m), 755 (m), 735 (s), 718 (m), 703 (m), 674 (m), 660 (m), 650 (s), 593 (w), 565 (m), 540 (m), 527 (w), 492 (w), 471 (m), 404 (m). **EA** ($C_8H_{14}CuN_{24}O_{10}$, 669.90) calcd: C 14.34, H 2.11, N 50.18%; found: C 14.27, H 2.36, N 49.87%. **BAM drophammer**: <1 J. **Friction tester:** 8 N. **ESD**: 160 mJ (at a grain size of 100–500 μm).

[Cu(ANIT)$_2$(1-AET)$_2$] (7)

The addition of 1-(2-azidoethyl)-1*H*-tetrazole (69.6 mg, 0.50 mmol, 2.0 eq.), dissolved in 5 mL of water to the aqueous solution of **1** (10 mL), yielded **7** (69.5 mg, 0.11 mmol, 44%). Precipitation according to General procedure B increased the yield to 71% (112.4 mg, 0.18 mmol). **DTA** (5 °C min^{-1}) onset: 159 °C (exothermic). **IR** (ATR, cm^{-1}): $\tilde{\nu}$ = 3326 (w), 3215 (w), 3143 (m), 2139 (m), 2114 (m), 2099 (m), 1640 (w), 1541 (vw), 1510 (m), 1473 (m), 1458 (m), 1437 (m), 1414 (s), 1397 (s), 1377 (m), 1348 (s), 1338 (s), 1309 (s), 1286 (vs), 1249 (vs), 1176 (s), 1159 (s), 1101 (vs), 1065 (w), 1022 (s), 1011 (s), 953 (w), 920 (m), 897 (s), 835 (m), 800 (w), 769 (m), 761 (m), 734 (m), 721 (w), 706 (m), 677 (s), 652 (s), 625 (m), 579 (w), 558 (m), 526 (m), 496 (m), 468 (m), 414 (w). **EA** ($C_8H_{14}CuN_{28}O_4$, 629.94) calcd: C 15.25, H 2.24, N 62.26%; found: C 15.04, H 2.41, N 61.77%. **BAM drophammer**: <1 J. **Friction tester:** 6 N. **ESD**: 20 mJ (at a grain size of <100 μm).

$[Cu(ANIT)_2(1\text{-}APT)_2]$ (8)

The addition of 1-(3-azidopropyl)-1*H*-tetrazole (76.6 mg, 0.50 mmol, 2.0 eq.), dissolved in 5 mL of water to the aqueous solution of **1** (10 mL), yielded **8** (111.9mg, 0.17 mmol). Therefore, it was obtained in a yield of 68%. **DTA** (5 °C min^{-1}) onset: 167 °C (exothermic). **IR** (ATR, cm^{-1}): $\tilde{\nu}$ = 3328 (w), 3250 (w), 3238 (w), 3197 (w), 3129 (w), 2116 (m), 2091 (m), 2069 (w), 2057 (w), 2048 (w), 2039 (w), 2032 (w), 2025 (w), 1609 (w), 1523 (m), 1511 (w), 1478 (m), 1462 (m), 1446 (w), 1423 (s), 1409 (s), 1385 (m), 1364 (w), 1329 (s), 1285 (s), 1249 (vs), 1217 (s), 1190 (m), 1157 (m), 1108 (m), 1092 (m), 1066 (w), 1024 (m), 994 (w), 969 (m), 915 (m), 885 (w), 849 (m), 829 (w), 819 (w), 783 (w), 776 (m), 762 (w), 743 (w), 734 (m), 714 (m), 680 (w), 665 (m), 655 (m), 613 (w), 600 (w), 563 (w), 536 (w), 488 (w), 484 (w), 466 (m), 412 (w). **EA** ($C_{10}H_{18}CuN_{28}O_4$, 657.99) calcd: C 18.25, H 2.76, N 59.60%; found: C 18.51, H 2.71, N 58.97%. **BAM drophammer**: <1 J. **Friction tester:** 20 N. **ESD**: 120 mJ (at a grain size of <100 μm).

$[Fe(ANIT)_2(H_2O)_2]\cdot 2H_2O$ (9)

NH_4ANIT (81.1 mg, 0.50 mmol, 2.0 eq.) was dissolved in 3 mL of deionized water and stirred at 60 °C. A solution of $FeSO_4\cdot 1.5H_2O$ (38.0 mg, 0.25 mmol) in 1 mL of water was then added dropwise under stirring for 10 minutes. The solution was allowed to cool to room temperature and stirred for 30 min, during which the precipitation of a beige solid occurred. The suspension was then filtered off, and washed with little water and EtOH before drying in air. Compound **9** was obtained in a yield of 68% (71.6 mg, 0.17 mmol). **DTA** (5 °C min^{-1}) onset: 118 °C (endothermic to exothermic transition). **IR** (ATR, cm^{-1}): $\tilde{\nu}$ = 3533 (m), 3353 (m), 3281 (m), 3069 (m), 1667 (w), 1644 (w), 1616 (w), 1521 (s), 1476 (s), 1435 (s), 1418 (m), 1367 (w), 1323 (s), 1279 (s), 1269 (s), 1175 (m), 1110 (m), 1078 (s), 1031 (w), 972 (w), 911 (w), 775 (m), 734 (s), 716 (s), 697 (s), 590 (vs), 530 (s), 509 (m), 457 (m), 419 (m), 405 (m). **EA** ($C_2H_{12}FeN_{14}O_8$, 416.05) calcd: C 5.77, H 2.91, N 47.13%; found: C 5.80, H 3.05, N 45.80%. **BAM drophammer**: 15 J. **Friction tester:** 288 N. **ESD**: 60 mJ (at a grain size of <100 μm).

Author contributions

Dr Maximilian Benz: writing – review & editing; Simon M. J. Endraß: writing – original draft, conceptualization, and investigation; Prof. Dr Thomas M. Klapötke: resources and funding acquisition; Dr Jörg Stierstorfer: supervision and writing – review & editing; Sadiq Strey: investigation.

Data availability

The data supporting this article have been included as part of the ESI.†

Deposition numbers 2394591 (for **1**), 2394593 (for **3**), 2394588 (for **4**), 2394623 (for **5a**), 2394590 (for **5b**), 2394592 (for **7**), 2394589 (for **8**), and 2394622 (for **9**) contain the supplementary crystallographic data for this paper.†

Software used for analysis and visualization has been cited in the documents.

Conflicts of interest

There are no conflicts to declare.

Acknowledgements

The authors gratefully acknowledge the financial support of this work by the Ludwig-Maximilians-Universität München. The authors would like to thank Marcus Lommel and Jan Cremers for their contribution to this work.

References

1 M. A. Ilyushin, I. V. Tselinsky and I. V. Shugalei, *Cent. Eur. J. Energ. Mater.*, 2012, **9**, 293–327.
2 Directive 2011/65/EU of the European Parliament and of the Council of 8 June 2011 on the restriction of the use of certain hazardous substances in electrical and electronic equipment, European Union, 2011.
3 Commission Delegated Directive (EU) 2021/647 of 15 January 2021 amending, for the purposes of adapting to scientific and technical progress, Annex III to Directive 2011/65/EU of the European Parliament and of the Council as regards an exemption for the use of certain lead and hexavalent chromium compounds in electric and electronic initiators of explosives for civil (professional) use, European Union, 2021.
4 M. H. V. Huynh, M. A. Hiskey, T. J. Meyer and M. Wetzler, *Proc. Natl. Acad. Sci. U. S. A.*, 2006, **103**, 5409–5412.
5 P. J. Landrigan, A. S. McKinney, L. C. Hopkins, W. W. Rhodes Jr, W. A. Price and D. H. Cox, *J. Am. Med. Assoc.*, 1975, **234**, 394–397.
6 D. R. S. Lima, M. L. S. Bezerra, E. B. Neves and F. R. Moreira, *Rev. Environ. Health*, 2011, **26**, 101–110.
7 M. S. Gruhne, M. Lommel, M. H. H. Wurzenberger, N. Szimhardt, T. M. Klapötke and J. Stierstorfer, *Propellants, Explos., Pyrotech.*, 2020, **45**, 147–153.
8 G. Geisberger, T. M. Klapötke and J. Stierstorfer, *Eur. J. Inorg. Chem.*, 2007, **2007**, 4743–4750.
9 J. W. Fronabarger, M. D. Williams, W. B. Sanborn, J. G. Bragg, D. A. Parrish and M. Bichay, *Propellants, Explos., Pyrotech.*, 2011, **36**, 541–550.
10 T. Wang, S. Bu, Z. Lu, B. Kuang, Z. Yi, Z. Xie, C. Zhang, Y. Li and J. Zhang, *Chem. Eng. J.*, 2023, **457**, 141267.
11 T. Wang, S. Bu, K. Wang, L. Zhang, Z. Yi, C. Zhang, W. Cao, S. Zhu and J. Zhang, *Chem. Eng. J.*, 2023, **452**, 139472.
12 T. Wang, Z. Lu, S. Bu, B. Kuang, L. Zhang, Z. Yi, K. Wang, S. Zhu and J. Zhang, *Def. Technol.*, 2024, **31**, 271–277.
13 K. D. Oyler, in *Green Energetic Materials*, 2014, pp. 103–132.

14 N. Szimhardt, M. H. H. Wurzenberger, A. Beringer, L. J. Daumann and J. Stierstorfer, *J. Mater. Chem. A*, 2017, **5**, 23753–23765.
15 M. H. H. Wurzenberger, N. Szimhardt and J. Stierstorfer, *Inorg. Chem.*, 2018, **57**, 7940–7949.
16 G. Lei, W. Cheng, Z.-J. Lu, T. Zhang, Z. Li and J. Zhang, *Mater. Horiz.*, 2023, **10**, 5775–5781.
17 O. Isayev, B. Rasulev, L. Gorb and J. Leszczynski, *Mol. Divers.*, 2006, **10**, 233–245.
18 J. A. Garrison and R. M. Herbst, *J. Org. Chem.*, 1957, **22**, 278–283.
19 N. Fischer, T. M. Klapötke, D. G. Piercey and J. Stierstorfer, *Z. Anorg. Allg. Chem.*, 2012, **638**, 302–310.
20 N. Fischer, T. M. Klapötke and J. Stierstorfer, *Z. Anorg. Allg. Chem.*, 2011, **637**, 1273–1276.
21 D. Fischer, T. M. Klapötke and J. Stierstorfer, *Eur. J. Inorg. Chem.*, 2015, **2015**, 4628–4632.
22 T. M. Klapötke, D. G. Piercey, N. Mehta, K. D. Oyler, M. Jorgensen, S. Lenahan, J. S. Salan, J. W. Fronabarger and M. D. Williams, *Z. Anorg. Allg. Chem.*, 2013, **639**, 681–688.
23 R. H. Muir, J. Bragg, A. Pearsall, M. Jorgensen, B. Sims, K. Yonoski, N. Mehta and J. S. Salan, *Org. Process Res. Dev.*, 2021, **25**, 1882–1888.
24 W. H. Gilligan and M. J. Kamlet, *US Department of Navy*, US4093623A, 1977.
25 D. D. Ford, S. Lenahan, M. Jörgensen, P. Dubé, M. Delude, P. E. Concannon, S. R. Anderson, K. D. Oyler, G. Cheng, N. Mehta and J. S. Salan, *Org. Process Res. Dev.*, 2015, **19**, 673–680.
26 M. Benz, T. M. Klapötke, J. Stierstorfer and M. Voggenreiter, *ACS Appl. Energy Mater.*, 2023, **1**, 3–6.
27 J. Schweifer, P. Weinberger, K. Mereiter, M. Boca, C. Reichl, G. Wiesinger, G. Hilscher, P. J. van Koningsbruggen, H. Kooijman, M. Grunert and W. Linert, *Inorg. Chim. Acta*, 2002, **339**, 297–306.
28 N. Szimhardt, M. H. H. Wurzenberger, T. M. Klapötke, J. T. Lechner, H. Reichherzer, C. C. Unger and J. Stierstorfer, *J. Mater. Chem. A*, 2018, **6**, 6565–6577.
29 P. J. Van Koningsbruggen, Y. Garcia, H. Kooijman, A. L. Spek, J. G. Haasnoot, O. Kahn, J. Linares, E. Codjovi and F. Varret, *J. Chem. Soc., Dalton Trans.*, 2001, 466–471.
30 M. S. Gruhne, T. Lenz, M. Rösch, M. Lommel, M. H. H. Wurzenberger, T. M. Klapötke and J. Stierstorfer, *Dalton Trans.*, 2021, **50**, 10811–10825.
31 M. H. H. Wurzenberger, M. S. Gruhne, M. Lommel, N. Szimhardt, T. M. Klapötke and J. Stierstorfer, *Chem. – Asian J.*, 2019, **14**, 2018–2028.
32 M. H. H. Wurzenberger, S. M. J. Endraß, M. Lommel, T. M. Klapötke and J. Stierstorfer, *ACS Appl. Energy Mater.*, 2020, **3**, 3798–3806.
33 O. V. Dolomanov, L. J. Bourhis, R. J. Gildea, J. A. K. Howard and H. Puschmann, *J. Appl. Crystallogr.*, 2009, **42**, 339–341.
34 G. M. Sheldrick, *Acta Crystallogr., Sect. A:Found. Adv.*, 2015, **71**, 3–8.
35 *SHELXL-97*, University of Göttingen, G. M. Sheldrick, Germany, 1997.
36 G. M. Sheldrick, *Acta Crystallogr., Sect. A:Found. Crystallogr.*, 2008, **64**, 112–122.
37 *Diamond – Crystal and Molecular Structure Visualization*, Crystal Impact, H. Putz and K. Brandenburg, Bonn, Germany.
38 Impact: insensitive >40 J, less sensitive ≥35 J, sensitive ≥4 J, very sensitive ≤3 J; Friction: insensitive >360 N, less sensitive = 360 N, sensitive <360 N and >80 N, very sensitive ≤80 N, extremely sensitive ≤10 N, According to: Recommendations on the Transport of Dangerous Goods, Manual of Tests and Criteria, 4th edn, New York-Geneva, 1999.
39 C. Zhang, T.-W. Wang, Z.-J. Lu, Z.-X. Yi, B.-L. Kuang, S. Bu, Z.-M. Xie, Y. Li, K. Wang and J.-G. Zhang, *J. Phys. Chem. C*, 2023, **127**, 12923–12930.
40 T.-W. Wang, Z.-J. Lu, Z.-X. Yi, Z.-M. Xie, L. Zhang, B.-L. Kuang, Y. Li and J.-G. Zhang, *Cryst. Growth Des.*, 2023, **23**, 5528–5534.
41 S. M. J. Endraß, T. M. Klapötke, M. Lommel, J. Stierstorfer, M. L. Weidemann and M. Werner, *ChemPlusChem*, 2024, **89**, e202400031.
42 T. M. Klapötke, *Energetic Materials Encyclopedia*, DeGruyter, Berlin/Boston, 2nd edn, 2021.
43 R. Matyáš and J. Pachman, in *Primary Explosives*, Springer Berlin Heidelberg, Berlin, Heidelberg, 2013, pp. 11–36.
44 A. J. Tulis, *J. Hazard. Mater.*, 1980, **4**, 3–10.
45 T. M. Klapötke, *Chemistry of High-Energy Materials*, De Gruyter, Berlin, Boston, 6th edn, 2022.